Analysis of coughed droplets using stereoscopic high-speed imaging

Adrian Roth*, Mehdi Stiti, Alexios Matamis, David Frantz, Mattias Richter, Marcus Alden and Edouard Berrocal

[1]Division of Combustion Physics, Department of Physics, Lund University, Lund, Sweden
*Corresponding author email: adrian.roth@forbrf.lth.se

Abstract
Droplets generated by talking and coughing play a major role in the spreading of COVID-19. Thus, there is a need for accurate measurements of the physical properties of exhaled droplets just at the exit of the mouth, including their number and velocity. Several challenges are associated with imaging coughed droplets. First, large variation of droplet size will translate to a large range of signal intensity when detected. Second, high droplet speed near the mouth requires both, short exposure time to freeze droplet motion and kHz recording rate to resolve their displacement. Finally, as a highly non-symmetrical spray system is formed from a cough, three-dimensional visualization is necessary to faithfully capture coughing events. Here, a 3D, high-speed imaging technique is presented that facilitates such challenging measurements. A laser beam with a rectangular cross-section (15 mm thick – 120 mm high) is formed and illuminates the imaged droplets exiting the mouth of a coughing person. The 3D droplet speed has been extracted over several coughs in order to draw statistical results where the maximum speed for a single cough has been estimated to vary between 12 and 36 m/s.

Keywords
Coughed droplets, COVID-19, high-speed laser sheet imaging, 3D velocity tracking.

Introduction

Different measures have been taken all around the world with the same goal: to reduce the spread of COVID-19. Examples of such measures are, social distancing and face covering. Multiple recent studies connect the disease transmission between humans, to droplets generated by talking, coughing and sneezing [1]. Nevertheless, some disagreement remains concerning the largest distance over which coughed droplets can spread the virus. Some studies show that this distance is larger than 6 m [2, 3], while others mention that the maximum spreading distance is about 1-2 m [4]. Analyzing, in detail, the transport and evaporation mechanisms of droplets ejected during coughing and talking is therefore extremely important for understanding host-to-host virus transmission and the spreading of viral diseases. The transport of the exhaled droplets in the environment depends on a large number of parameters such as the size and three-dimensional velocity as well as the motion of the surrounding air (such as ventilation). In order to determine precisely these different parameters, it is necessary to rely on experimental evidences.

Measurements applied for characterizing coughs usually rely on imaging techniques that give information of the air flow-field shape and propagation. In order to visualize this field during the cough phase, high-speed photography is commonly used [5, 6] since it has a high enough temporal resolution. Visualization can be made either by shadowgraph techniques, or with the use of tracers, such as smoke that tags the flow and can be captured by one or more high-speed cameras. Another approach is to use Schlieren [7, 8, 9]. This technique takes advantage of the generally higher temperature of the air flow generated when coughing compared to that of the ambient air and then the generated images depict the variation of the refractive index during the coughing phase. Finally, the Particle Image Velocimetry (PIV) technique has been

implemented on coughs [8, 10, 11, 12, 13, 14]. The technique usually apply illumination of the mentioned tracer particles with a laser plane generated by a pulsed laser. The light scattered by the tracers is then captured by a camera synchronized to two laser pulses and from the images the tracer particle displacement can be estimated. Here, only the reconstruction of the particle velocity field in the laser plane is possible. With PIV, parameters such as the flow propagation, front velocity or spreading angle can be extracted. In the literature, this spreading angle for coughing varies between 23° and 36° [5, 6, 8, 12] and the droplet maximum speed varies between 3.2 and 28.8 m/s [5, 6, 8, 7, 10, 11, 12, 14]. Recently Simha et al. [4] found a maximum speed of around 6 m/s near the mouth exit and a decrease of 0.2 m/s 2.5 m away from the mouth. They also proposed a universal exponentially decaying distance–speed trend to obtain the airflow speed at large distances.
To understand how virions that are encapsulated in droplets are transported from host-to-host it is necessary to implement imaging techniques that provide temporally resolved information of the velocity of the droplets. In this work, we propose a technique that makes use of two high-speed cameras to detect the scattered light from droplets crossing a laser sheet. With this stereoscopic arrangement, the 3D position and velocity of the droplets are obtained using a 3D Particle Tracking Velocimetry (PTV) approach. The next section describes the experimental setup followed by information of how the 3D PTV works. Then, the found droplet counting and velocities are shown and discussed finalized by the conclusions of this work.

Experimental setup

To detect and estimate the velocity of coughed droplets, this work used two high-speed cameras and two continuous wave lasers. The two laser beams were combined using a dichroic mirror and then formed into a laser sheet with a size of 15 mm x 120 mm as illustrated in Figure 1a and b. Then, a person positioned around 20 mm above the sheet, coughed droplets downward that scatters the laser light into the cameras when crossing the sheet. The use of two lasers enabled the detection of smaller droplets. Laser power outputs were 4 W and 5 W with wavelengths of 450 nm and 532 nm respectively. The scattered light was collected by two Phantom VEO 710L high-speed cameras from LaVision Research, running at 15 000 frames per second. The exposure time was set to 50 µs that allowed for each cough event to be resolved temporally, while optimizing the detected light signal. Each recording lasted around 2 seconds which was sufficient to capture two or three successive coughs. To be able to detect even smaller drops the cameras were set at an angle of 54° to the laser direction, see Figure 1b. By using this setup, instead of an orthogonal angle of 90°, the imaged intensity is more than 20 times larger. This angle, together with the usage of two lasers, resulted in detection of droplets as small as 8 µm. Finally, to get the 3D positions of detected droplets, the cameras have been set up in a stereoscopic configuration. The methods for extracting the 3D positions and also droplet velocities are explained in the next section.

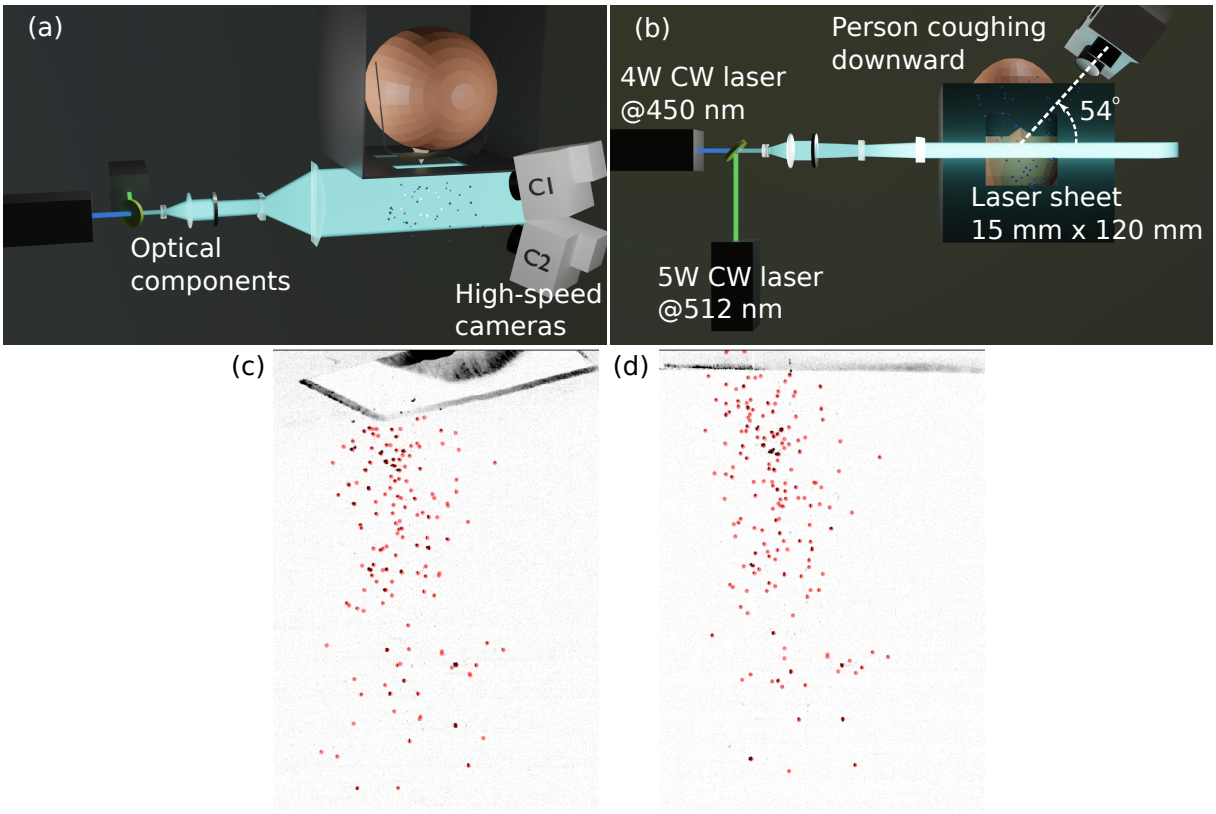

Figure 1. Illustration of the experimental setup. (a) is from the side and (b) is from the bottom. In (c) and (d) an example of recorded images is shown for camera C1 and C2 respectively. Here, the detected droplets in the light sheet are represented as red dots.

Extraction of droplet 3D velocity

The velocity of coughed droplets is obtained through a post-processing scheme divided into three steps:

1. Finding the droplet coordinates in the images of each camera,
2. 3D triangulate the droplet positions with a camera calibration
3. Use 3D Particle Tracking Velocimetry (3D-PTV) to extract droplet tracks together with droplet velocities.

Figure 2 presents an example of post-processing results.

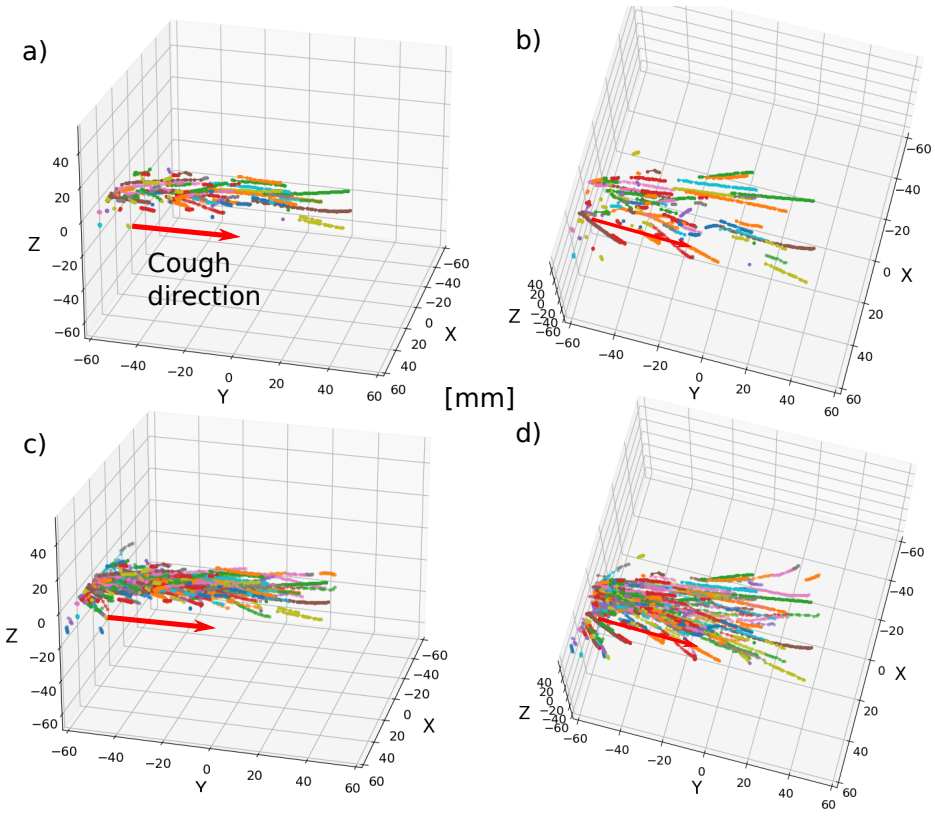

Figure 2. Example of post-processing results. Panel (a) and (b) show the final 3D tracks at a single time and from two different angles. The general cough direction is indicated by the red arrows as the positive Y-axis. Panels (c) and (d) show accumulated particle tracks for the first half of time in a single cough. One can see how the particles are not just traveling in the cough direction but also spreading.

First the droplet coordinates in the images should be estimated. From the raw images, the average background intensity is subtracted, pixels that include corrupting reflection of laser light are masked and finally a global intensity threshold is applied to detect and isolate the imaged droplets. All pixels with a value above 30 counts in the 12 bit images are defined as droplets. After the threshold, the found image areas are defined as droplets. To get the droplet coordinates in the images, the weighted average of the pixel intensities and pixel coordinates in the collected areas are used.

Having obtained droplet image coordinates from the cameras, it is possible to perform the second step and triangulate the 3D position of each particle. In order to achieve this, a camera calibration is required. In this work, the calibration scheme suggested by Machicoane et al. [15] has been used. This scheme, in contrast to the classical pinhole camera matrix approach, estimates a correspondence between each pixel and a 3D line describing the light ray that, after the imaging lenses, will be found at the pixel location in the sensor. Here, different distortions that the image system inhabit can be taken into account without explicitly modeling them. To estimate these lines, a known pattern (here a checkerboard pattern with 19x10 intersections) is put on a rail. The world coordinate system is here defined so that only the third dimension Z is changed while the X and Y are kept constant for the pattern. Then, images are recorded while moving the pattern to known locations on the rail. We used 16 different steps from Z=0 to Z=15 mm. Since the pattern is known, we can for each location find multiple (in our case 190) point-correspondences between camera coordinates and world coordinates for the pattern. With these correspondences, the coefficients for a 2D polynomial transform can be estimated that goes from the camera (x, y) coordinates to the world (X, Y). By making this transform of an order 2 or higher, imaging distortions are taken into account. This transform can now be used to get world (X, Y) coordinates for each pixel in each Z-location. Meaning, that each pixel has multiple 3D world points (in out case 16) where all points should be on the 3D line of the light ray

that is imaged by this pixel. Finally, the 3D line is estimated by a total least squares algorithm for each pixel. The drawback of this scheme is the requirement to use a rail or in some other way know the coordinates and orientation of all patterns compared to the classical pinhole method [16] where only a single pattern at arbitrary orientation is required. This scheme is, however, as mentioned more versatile when it comes to taking lens distortions into account.
The next processing step is to use this calibration to estimate droplet 3D coordinates. Since all droplet image coordinates for each camera are now connected to a 3D line, we know that the 3D droplet should be found somewhere on or close to this line. The lines are then cross compared for all droplets found in camera one and two and for one combination of a line from the first and second camera there is a single position where the lines are closest to one another. At this position, the distance between the lines is the matching error. The two particles with the smallest error are found as an attempted match. Then, only if the matching error is below a threshold (0.5 mm is used in this work) the 3D coordinates of the droplet is estimated as the center between the points on the lines that are the closest together. This process is repeated until the matching error exceeds the threshold.
Finally, with known 3D coordinates of droplets, it is possible to extract velocities by tracking the droplets between frames. The 3D-PTV tracking algorithm used here is similar to the one suggested by Clark et al. [17] that have an approach based on an algorithm called the Four Frame best estimate [18]. This algorithm tries for each track and point in time to use an estimate of its current velocity and acceleration to extrapolate where the particle should end up in future frames. This information is used to choose the most likely particle to continue the track. In addition, Clark et al. suggests to recursively try all possible next particles (within predefined bounds) to find the optimal track. The same approach is used in this work where the longest final track is returned in each recursive step to find the optimal track. With the tracks, the differences between coordinates in two consecutive frames is used to estimate the particle velocity.

Results and discussion

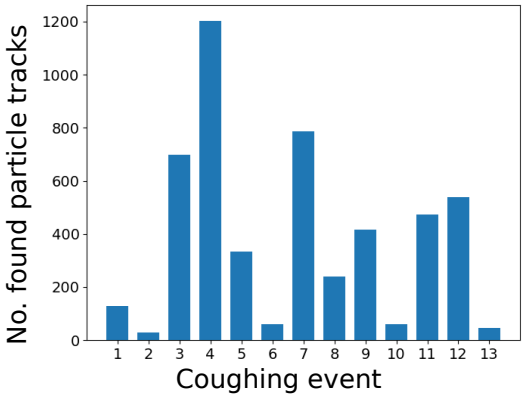

Figure 3. Bars showing the number of tracked particles for each cough event.

The data that has been analyzed in this work is from 13 different coughs produced by a single healthy person. The detected droplets expelled during each cough have been triangulated in 3D and then tracked following the scheme presented in the previous section. Our main results are the found speed quantities of the tracked droplets with an additional counting of how many droplets were found. Here, the speed is calculated with the Euclidian norm of the velocity vector as,

$$s = \sqrt{\Delta \mathrm{X}^2 + \Delta \mathrm{Y}^2 + \Delta \mathrm{Z}^2}/\Delta \mathrm{t} \tag{1}$$

where the Δ represent the difference in droplet coordinate values between two consecutive

frames and the Δt is the time between the frames.
The number of tracked droplets for each cough are shown in Figure 3. As observed, this number varies greatly between different coughs. The reason for this is probably a combination of how coughs naturally produce different number of droplets (depending on the saliva production, coughing strength etc.) together with changes in how the cough was aimed relative to the laser sheet. The second reason is connected to that the participant was given some mobility in order to cough in the most natural way possible during the experiments. This resulted in slightly different direction of the coughs that can give a significant difference in detected droplets since the laser sheet is so thin. This is one of the main trade offs with this experimental setup. It is both desired to have a large laser sheet to detect droplets in a large volume and a high laser power concentration to be able to detect small droplets.
We first consider the cough with the most tracked droplets (cough number 4 in Figure 3) with results shown in Figure 4. A histogram of the estimated speeds are shown in panel (a) where mainly speeds below 18 m/s are found with a maximum speed of 24 m/s. Figure 4b represents the speed field profile in the XY plane of this cough. To produce the plot, all speeds found at coordinates inside each of the XY boxes are averaged to get a value. The white boxes represent areas with no tracked particles. One can from this map see the main jet of the cough with higher speeds compared to the surrounding slower droplets. Figure 4c shows the speed over time. Here, the time was divided into different bins with a width of 6 ms, The average and standard deviation of all speeds within each bin gives the center and error bar on the blue line. One can notice how the average speed decreases from 10 to 2 m/s in the first 50 ms showing that the fastest droplets in this cough are ejected within this time frame.

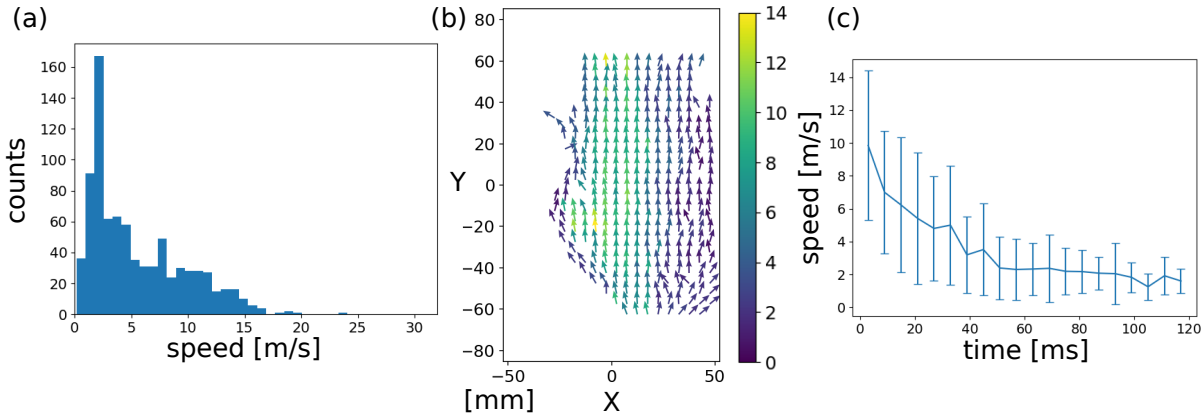

Figure 4. Resulting speeds for a single cough with around 1200 tracked droplets. (a) shows a histogram of all tracked droplet speeds in this cough. (b) shows the droplet speed profile in the XY plane and (c) shows how the droplet velocity is changing over time and how much it is varying within each time bin.

In addition to analyzing a single cough, it is possible to analyze statistics for all coughs which is presented in Figure 5. In panel (a), a histogram of all tracked droplet speeds is shown where the average speed is found to be 5.4 m/s and the maximum speed is around 31 m/s. If instead one looks at the maximum speed for individual coughs (panel (c)) it varies between 9 and 31 m/s where only cough event 2 has max speed below 15 m/s and event 8, 9 and 12 above 28 m/s. Coughing event 2 also has very few found tracks which might be connected to the low maximum speed. One should note here that there are few examples of the largest speeds and these particular tracks might have been found in error by the algorithm. The false positive rate of found tracks should be analyzed in the future to correct for these possibly false tracks. In (b) of the same figure, the XY speed profile is shown. One can notice a possible jet center in this profile where the speed is decreasing with larger distance from this center. Though, compared to the single cough profile, it is harder to find an obvious center of the coughed jet and this can be connected to the mentioned changes in coughing direction between the coughs. A solution in the future would be to align all coughs to have their respective jets in the same

location and with the same direction before merging for improved statistics. As mentioned one important property of the coughed droplet is to estimate their deceleration over distance and time. This together with the maximum velocity will then enable the estimation of how far droplets can travel before touching the ground and in extension how far virions can travel by coughed droplets. From the result in Figure 5b a deceleration can possibly be observed within the 120 mm distance in the Y dimension that is measured. However, to quantify this deceleration the improvements mentioned above should be implemented and more data should be analyzed for different persons to get statistically rigorous results.

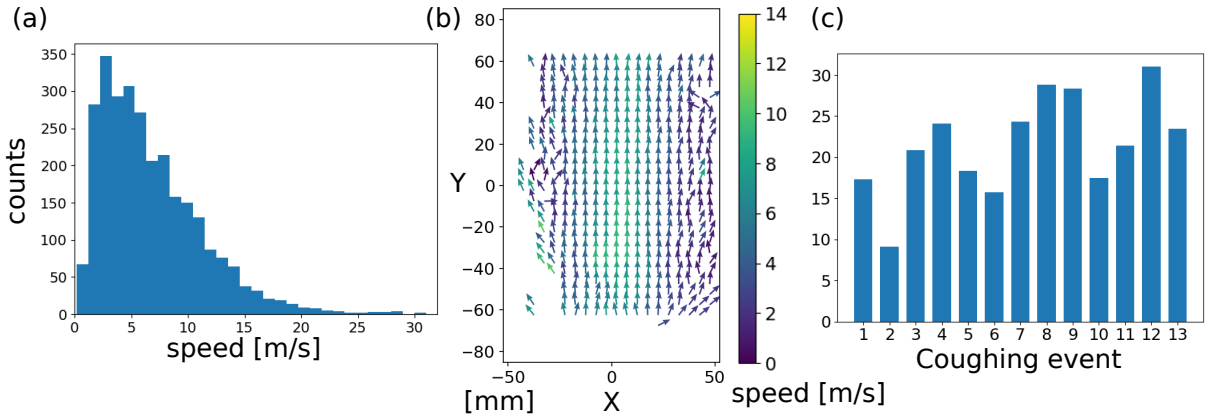

Figure 5. Resulting speeds for all tracks in all 13 coughs. The panels are similar to Figure 4 with speed histogram in panel (a), XY speed profile in (b). In panel (c) is the maximum tracked droplet speed for each coughing event (same as Figure 3).

Conclusions

In this work, the 3D speed of coughed droplets has been investigated. The work is based on experiments with stereo high-speed imaging of scattered laser light from droplets. The average speed of the droplets was found to be 5.4 m/s with maximum speeds for coughs varying between 9 and 31 m/s. The experimental data obtained using this technique can in the future be used to analyze coughs from different persons and compare similarities and differences between how different people cough. In addition, one can simulate droplet trajectories further away from the mouth with the use of measured velocities from these results. Here, an objective is to obtain a general law of trajectories of the droplets expelled during the coughing phase. To derive and verify this law, the coughed droplets can also be recorded at greater distances from the mouth than those studied here. This research will give important information to determine the social safety distances that should be put in place in order to limit the spread of disease by coughed droplets.

Acknowledgements

The authors would like to thank for the financial support from the European Research Council (ERC - 638546) and the Swedish Research Council (Vetenskapsrådet 2016-03894).

Nomenclature

s	Speed [m/s]
X, Y, Z	Coordinates [mm]

References

[1] Annie L Zhang, Yuan Wang, and Mario J Molina. Erratum: Identifying airborne transmission as the dominant route for the spread of COVID-19 (Proceedings of the National Academy of Sciences of the United States of America (2020) 117 (14857-14863) DOI:

10.1073/pnas.2009637117). *Proceedings of the National Academy of Sciences of the United States of America*, 117(41):25942–25943, 2020.

[2] Lydia Bourouiba. Turbulent Gas Clouds and Respiratory Pathogen Emissions Potential Implications for Reducing Transmission of COVID-19. *JAMA*, 323(18):2020–2021, 2020.

[3] Hongying Li, Fong Yew Leong, George Xu, Zhengwei Ge, Chang Wei Kang, and Keng Hui Lim. Dispersion of evaporating cough droplets in tropical outdoor environment. *Physics of Fluids*, 32(11), 2020.

[4] Padmanabha Prasanna Simha and Prasanna Simha Mohan Rao. Universal trends in human cough airflows at large distances. *Physics of Fluids*, 32(8), 2020.

[5] Lydia Bourouiba, Eline Dehandschoewercker, and John W.M. Bush. Violent expiratory events: On coughing and sneezing. *Journal of Fluid Mechanics*, 745:537–563, 2014.

[6] J. K. Gupta, C. H. Lin, and Q. Chen. Flow dynamics and characterization of a cough. *Indoor Air*, 19(6):517–525, 2009.

[7] Julian W. Tang, Thomas J. Liebner, Brent A. Craven, and Gary S. Settles. A schlieren optical study of the human cough with and without wearing masks for aerosol infection control. *Journal of the Royal Society Interface*, 6(SUPPL. 6):727–736, 2009.

[8] Julian W. Tang, Andre Nicolle, Jovan Pantelic, Gerald C. Koh, Liang de Wang, Muhammad Amin, Christian A. Klettner, David K.W. Cheong, Chandra Sekhar, and Kwok Wai Tham. Airflow dynamics of coughing in healthy human volunteers by shadowgraph imaging: An aid to aerosol infection control. *PLoS ONE*, 7(4), 2012.

[9] Manouk Abkarian, Simon Mendez, Nan Xue, Fan Yang, and Howard A. Stone. Speech can produce jet-like transport relevant to asymptomatic spreading of virus. *Proceedings of the National Academy of Sciences of the United States of America*, 117(41):25237–25245, 2020.

[10] Meg Vansciver, Shelly Miller, and Jean Hertzberg. Particle image velocimetry of human cough. *Aerosol Science and Technology*, 45(3):415–422, 2011.

[11] Eric Savory, William E. Lin, Karin Blackman, Matthew C. Roberto, Lauren R. Cuthbertson, James A. Scott, and Samira Mubareka. Western Cold and Flu (WeCoF) aerosol study - Preliminary results. *BMC Research Notes*, 7(1):1–11, 2014.

[12] Soon Bark Kwon, Jaehyung Park, Jaeyoun Jang, Youngmin Cho, Duck Shin Park, Changsoo Kim, Gwi Nam Bae, and Am Jang. Study on the initial velocity distribution of exhaled air from coughing and speaking. *Chemosphere*, 87(11):1260–1264, 2012.

[13] Shengwei W. Zhu, Shinsuke Kato, and Jeong Hoon Yang. Study on transport characteristics of saliva droplets produced by coughing in a calm indoor environment. *Building and Environment*, 41(12):1691–1702, 2006.

[14] C. Y.H. Chao, M. P. Wan, L. Morawska, G. R. Johnson, Z. D. Ristovski, M. Hargreaves, K. Mengersen, S. Corbett, Y. Li, X. Xie, and D. Katoshevski. Characterization of expiration air jets and droplet size distributions immediately at the mouth opening. *Journal of Aerosol Science*, 40(2):122–133, 2009.

[15] N. Machicoane, A. Aliseda, R. Volk, and M. Bourgoin. A simplified and versatile calibration method for multi-camera optical systems in 3D particle imaging. *Review of Scientific Instruments*, 90(3):035112, March 2019.

[16] R. Tsai. A versatile camera calibration technique for high-accuracy 3d machine vision metrology using off-the-shelf tv cameras and lenses. *IEEE Journal on Robotics and Automation*, 3(4):323–344, 1987.

[17] A Clark, N Machicoane, and A Aliseda. A quantitative study of track initialization of the four-frame best estimate algorithm for three-dimensional Lagrangian particle tracking. *Measurement Science and Technology*, 30(4):045302, April 2019.

[18] Nicholas T. Ouellette, Haitao Xu, and Eberhard Bodenschatz. A quantitative study of three-dimensional Lagrangian particle tracking algorithms. *Experiments in Fluids*, 40(2):301–313, February 2006.